



Formability and microstructure of TC4 titanium alloy hollow shafts formed by cross-wedge rolling with a mandrel

Pengni Feng¹ · Cuiping Yang^{1,2} · Baoyu Wang^{1,2} · Junling Li¹ · Jinxia Shen¹ · Xiaoming Yang¹

Received: 5 September 2020 / Accepted: 12 January 2021 / Published online: 15 March 2021
© The Author(s), under exclusive licence to Springer-Verlag London Ltd. part of Springer Nature 2021

Abstract

The formability and microstructure of TC4 titanium alloy hollow shafts formed by cross-wedge rolling (CWR) are being investigated to ensure that products manufactured for utilisation in the aviation sector are lightweight. The flow behaviour of the TC4 alloy was studied via isothermal hot compression tests. The constitutive equations in different phase regions were then established and applied to a finite element (FE) model to study the effect of process parameters on the ellipticity of the TC4 alloy hollow shafts formed by CWR. Corresponding CWR experiments were conducted to validate the FE model; further, the microstructure of the TC4 alloy hollow shafts was investigated. The results demonstrate that forming angle, stretching angle and area reduction considerably affect the ellipticity of the TC4 alloy hollow shafts by varying the contact area between a die and a workpiece. The ellipticity evidently increases as the relative wall thickness decreases, as the flattening deformation increases. An increase in the deformation temperature will result in a decrease in the deformation resistance of the TC4 alloy and an increase in the ellipticity. Moreover, the effect of the deformation temperature, area reduction and wall thickness of the workpiece on the microstructure of the TC4 alloy hollow shafts formed by CWR was investigated. The degree of kink or globularisation of the strip alpha phase increases with the above parameters. The volume fraction of the beta phase increases with the deformation temperature. The microstructure is typically equiaxed when the deformation temperature is 950 °C.

Keywords TC4 titanium alloy · Cross-wedge rolling · Hollow shafts · Ellipticity · Microstructure

1 Introduction

Lightweight structures are extremely important in the aircraft industry. Hollow shafts are well suited to satisfy the requirements of such lightweight structures, under the premise of ensuring satisfactory performance. Titanium alloy is commonly used in aerospace owing to its low density, high specific strength and excellent corrosion resistance. As the most widely used titanium alloy, TC4 alloy is an ideal aircraft structural component [1]. Therefore, developing and utilising TC4

titanium hollow shafts in aviation products will be of great significance. At present, the major technologies utilised for the manufacture of titanium shafts are forging and hot extrusion. Nevertheless, owing to the narrow temperature range of forging titanium and the large deformation resistance of titanium, the uniformity of the microstructure of the workpiece cannot be guaranteed when traditional processes are used. Employing these processes can seriously affect the performance of the workpiece and even induce cracks [2]. Cross-wedge rolling (CWR) [3] is an efficient near-net-shape process employed to manufacture shaft parts. Uniform plastic deformation of cylindrical billets is caused by the continuous rotating motion of wedge tools; this feature helps improve the quality of the shaft parts and effectively reduces the manufacturing cost. Thus, in this study, the forming technology of the TC4 alloy hollow shafts formed by CWR has been investigated.

Thus far, a sufficient amount of research has been conducted on CWR hollow shafts. Bartnicki et al. [4] analysed the stability of the formed hollow shafts via flat CWR and studied the relationships between the process

✉ Baoyu Wang
bywang@ustb.edu.cn

Pengni Feng
pnfeng1122@163.com

¹ School of Mechanical Engineering, University of Science and Technology Beijing, Beijing 100083, China

² Beijing Laboratory of Metallic Materials and Processing for Modern Transportation, Beijing 100083, China

Table 1 Main chemical composition of the raw TC4 alloy

Element	Mass fraction (%)
Al	6.2–6.3
V	4.2–4.3
Y	< 0.001
Fe	0.05–0.06
C	0.01–0.02
N	0.02
H	0.004
O	0.17–0.18
Ti	bal

stability, deformation ratio and wall thickness of the formed workpiece. Bartnicki et al. [5] also numerically simulated the forming process of hollow shafts via three-rolls CWR. Ding et al. [6] investigated the influence of process parameters on the ellipticity of hollowed shafts formed via CWR using a finite element (FE) simulation. Yang et al. [7] analysed the effect of the flattening deformation on the hollow shafts formed via CWR and proposed to reduce the flattening deformation by selecting a small forming angle and stretching angle of the tools. Yang et al. [8] also researched the ellipticity of AISI 1045 steel hollow shafts in CWR with a mandrel and developed the axle sleeves of trucks with high forming quality. Ji et al. [9, 10] investigated the ellipticity and swollen hole of the hollow valves and proposed a method for manufacturing 4Cr9Si2 hollow valves via CWR without mandrel and forging. Huang et al. [11] studied the influence of the mandrels with different relative diameters on the forming quality of the hollow shafts of 40MnBH formed via CWR through numerical simulations and experimental trials. Nowadays, materials, other than steel, formed via CWR are gradually being explored. Urankar

et al. [12] developed the failure conditions for the hollow shafts of Aluminum 6061 T6 and 4140 Tool Steel formed via CWR; further, they predicted the operating conditions of failure by introducing a dimensionless crushing parameter. Moreover, Urankar et al. [13] determined the critical friction values in the CWR of hollow shafts of Aluminum 6061 T6 using an explicit dynamic FE method and specialised experiments. Çakırcalı et al. [14] studied the CWR deformation and fracture of Ti6Al4V alloy solid billets based on a coupled thermo–mechanical FE model analysis. Li et al. [15, 16] numerically and experimentally studied the effect of the CWR parameters on sintering TC4 alloy blade preforms and stated that both the tool parameters and rolling temperature substantially affect the formability of the TC4 alloy. Li et al. [17] also studied the effects of the CWR parameters on the TC6 alloy by establishing a coupled thermo–mechanical and microstructural FE model.

The existing studies on the CWR of hollow shafts focused on the use of various steels. Further, in the CWR of titanium alloy, solely solid products were used. In this study, the formability and microstructure of the TC4 titanium alloy hollow shafts formed by CWR with a mandrel were investigated. The constitutive equations of the TC4 alloy in different phase regions were derived via isothermal hot compression tests. These equations were then applied to the FE model to investigate the influence of process parameters on the ellipticity of the TC4 alloy hollow shafts formed by CWR. The corresponding CWR experiments were conducted to validate the FE model; further, the microstructure of the TC4 alloy hollow shafts formed by CWR was investigated.

2 Deformation behaviour of TC4 alloy

2.1 Materials and experimental procedure

The material employed in this experiment is a TC4 alloy hot-rolled bar. Table 1 summarises the main chemical composition of this material. The initial microstructure comprises a matrix alpha phase and a small amount of residual beta phase, which exhibits the structural characteristics of a strip-like processing state; further, a part of the alpha phase is elongated into strip alpha phase, as shown in Fig. 1. The volume fraction of the alpha phase is approximately 80% and the beta transus temperature is approximately 990 °C.

The true stress–strain curves of the TC4 alloy were obtained via the isothermal compression tests. The diameter and height of the cylindrical specimens, which were made from the rolled bar, were 8 mm and 12 mm, respectively. According to the beta transus temperature and the characteristics of CWR, the deformation temperatures and strain rates were determined to be in the range 850–1050 °C and 0.1–10 s⁻¹,

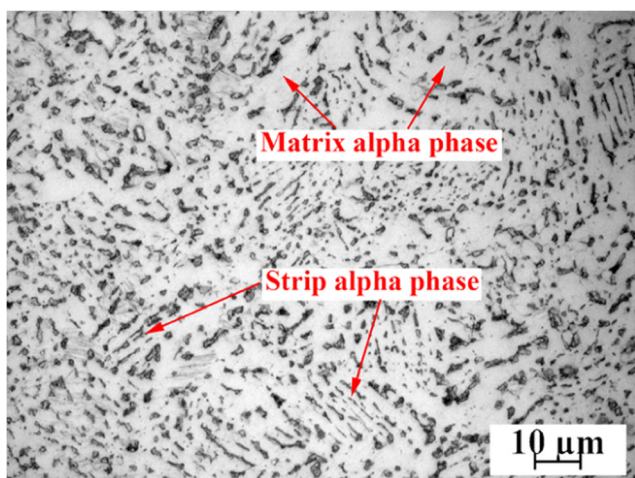
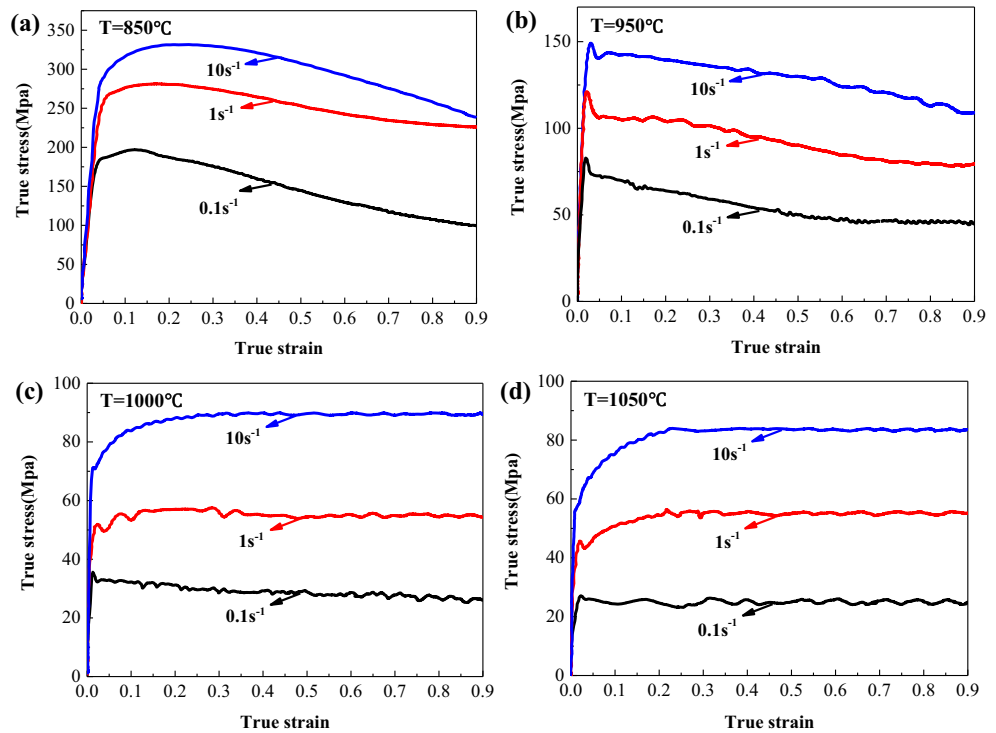
**Fig. 1** Initial microstructure of the raw TC4 alloy

Fig. 2 True stress–true strain curves for the TC4 alloy measured at **a** 850 , **b** 950 , **c** 1000 and **d** 1050



respectively; further, a 60% reduction in the height of the specimens was observed.

2.2 Flow behaviour

When the deformation temperature is lower than the beta transus temperature, the microstructure of the TC4 alloy comprises both the alpha and beta phases, which is in the two-phase region. When the temperature exceeds the beta transus temperature, all of the alpha phase is transformed into beta phase; further, the microstructure of the TC4 alloy is composed of the beta phase, which is in the single-phase region [18]. The typical true stress–strain

curves of the TC4 alloy in the two-phase region (850–950 °C) and single-phase region (1000–1050 °C) are shown in Fig. 2. The peak stress decreases as the deformation temperature increases and the strain rate decreases. The flow stress increases sharply at the initial deformation stage because of the influence of the hardening of the workpiece. Compared with that in the single-phase region, the flow behaviour of the TC4 alloy in the two-phase region exhibits an evident softening characteristic during the subsequent deformation process. The transformation from the hard alpha phase to the soft beta phase can cause softening of the flow [19]. Further, the globularisation of

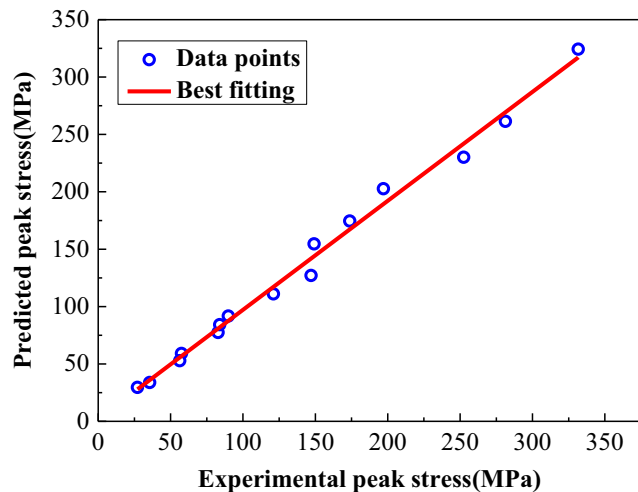


Fig. 3 Comparison of predicted peak stress and experimental peak stress



Fig. 4 Forming wedge tools of $\alpha = 31^\circ$ and $\alpha = 38^\circ$ with the same $\beta = 4^\circ$

Table 2 CWR process parameters of FE simulation

$\alpha(^{\circ})$	$\beta(^{\circ})$	t_r	$\varphi(\%)$	$T()$
31, 38, 45	4	0.43	45	900
38	2.5, 4, 5.5	0.43	45	900
38	4	0.36, 0.43, 0.50	45	900
38	4	0.43	30, 45, 60	900
38	4	0.43	45	850, 900, 950, 1050

the alpha platelets or the lamellar secondary alpha phase in the two-phase region can also lead to softening of the flow of titanium alloy [20]. In this study, the kink and globularisation of the strip alpha phase can soften the flow of the TC4 alloy, which will be discussed in Section 4.3.

2.3 Determination of the constitutive equation

To more clearly illustrate the thermal deformation mechanism of the TC4 alloy, this study employs the classical Arrhenius-type constitutive equation to express the relationship among the flow stress, strain rate and deformation temperature, as follows:

$$\dot{\epsilon} = \begin{cases} A_1 \sigma^{n_1} \exp[-Q/(RT)] & k\sigma < 0.8 \\ A_2 \exp(m\sigma) \exp[-Q/(RT)] & k\sigma > 1.2 \\ A [\sinh(k\sigma)]^n \exp[-Q/(RT)] & \text{for all } \sigma \end{cases} \quad (1)$$

where $\dot{\epsilon}$ represents the strain rate (s^{-1}); σ , the flow stress(MPa); Q , the activation energy of the hot deformation ($J \cdot mol^{-1}$); R , the molar gas constant ($8.3145 J \cdot mol^{-1} \cdot K^{-1}$); and T , absolute temperature (K). A_1, A_2, A, n_1, n, k and m are the material constants, and $k = m/n_1$.

The Zener–Hollomon parameter, which represents the compensation of the deformation temperature corresponding to strain rate, is given as follows:

$$Z = \dot{\epsilon} \exp[-Q/(RT)] = A [\sinh(k\sigma)]^n \quad (2)$$

Each material constant was determined in accordance with the peak stress under different conditions of the compression tests via a series of calculations. The constitutive equations of the TC4 alloys in different phase regions were finally derived as follows:

$$\dot{\epsilon} = 4.8073 \times 10^{33} [\sinh(0.0059\sigma)]^{5.8189} \exp[-767443/(RT)] \quad \text{two-phase region} \quad (3)$$

$$\dot{\epsilon} = 2.4148 \times 10^5 [\sinh(0.0184\sigma)]^{3.3544} \exp[-141043/(RT)] \quad \text{single-phase region} \quad (4)$$

Correspondingly, the Z parameters of the TC4 alloy in different phase regions were solved as follows:

$$Z = \dot{\epsilon} \exp[-767443/(RT)] \quad \text{two-phase region} \quad (5)$$

$$Z = \dot{\epsilon} \exp[-141043/(RT)] \quad \text{single-phase region} \quad (6)$$

Fig. 5 a FE model and b forming process of the TC4 alloy hollow shaft in CWR with a mandrel

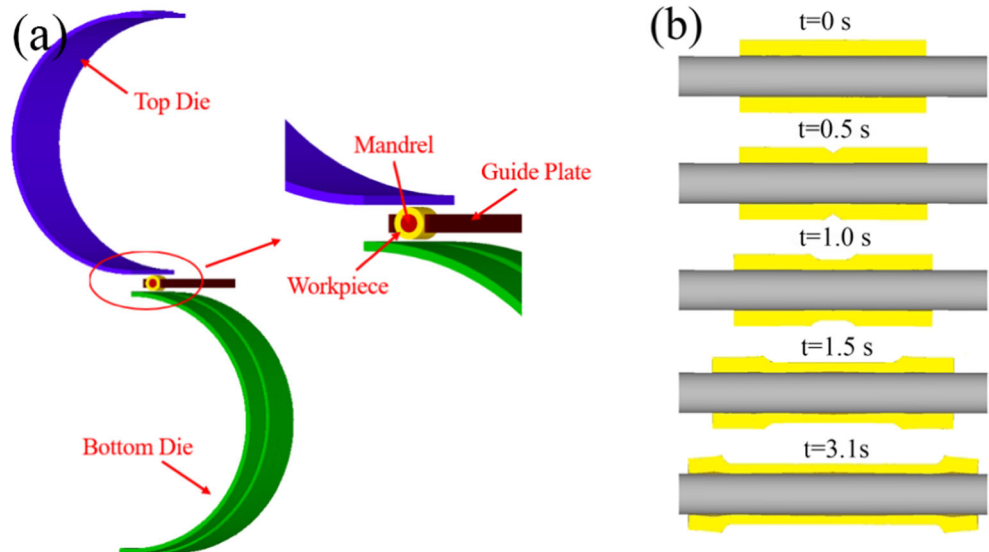


Table 3 Parameters of the CWR simulation

Parameter	Value
Temperature of tools (°C)	20
Temperature of environment (°C)	20
Contact heat transfer coefficient (W·m ⁻² ·K ⁻¹)	20×10 ³
Convection coefficient (W·m ⁻² ·K ⁻¹)	20
Coefficient of mechanical energy to heating	0.9
Emissivity	0.7
Speed of roll (rpm)	10
Friction factor between workpiece and die	0.9
Friction factor between workpiece and guide plate	0.3

The constitutive equations will be applied for the FE simulation of the TC4 alloy hollow shafts formed via CWR. Therefore, to assess the dependability of the equations, the correlation coefficient (RR) and average absolute relative error (AARE) were introduced, as follows:

$$RR = \frac{\sum_{i=1}^N (E_i - \bar{E})(P_i - \bar{P})}{\sqrt{\sum_{i=1}^N (E_i - \bar{E})^2 \sum_{i=1}^N (P_i - \bar{P})^2}} \quad (7)$$

$$AARE = \frac{1}{N} \sum_{i=1}^N \left| \frac{E_i - P_i}{E_i} \right| \times 100\%$$

where E_i and P_i represent the experimental and predicated flow stress; further, \bar{E} and \bar{P} represent the average experimental and predicated flow stress. By solving Eq. (7), RR of 0.9958 and AARE of 5.246% are obtained, which indicates that the established TC4 constitutive equations have high

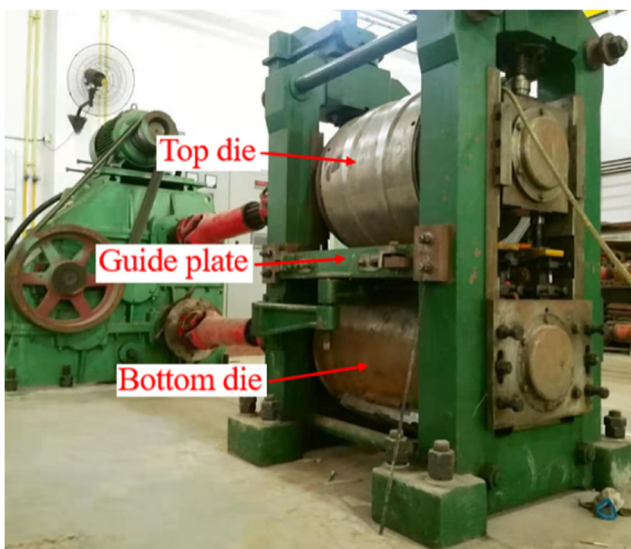


Fig. 6 Experimental H630 mill equipment

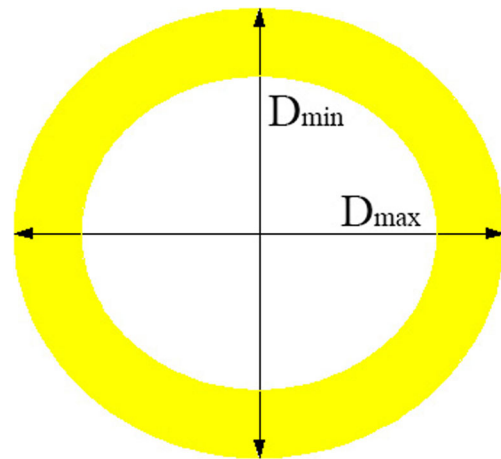


Fig. 7 Schematic of ellipticity of cross-section

prediction accuracy. The predicted peak stress and experimental peak stress under different deformation conditions are compared in Fig. 3.

3 FE simulation and CWR experiments

3.1 Choosing the simulation parameters

In this study, the effects of CWR process parameters on the formability and microstructure of the TC4 alloy hollow shafts were studied numerically and experimentally based on the single-factor design. The forming angles (α) and stretching angles (β) are selected to be in the range 31–45° and 2.5–5°, respectively. Figure 4 shows the forming wedge tools at forming angles of 31° and 38° at the same stretching angle of 4°. The initial outer diameter D_0 of the billet is 35 mm. The area reduction φ and the relative wall thickness t_r of the hollow billet are defined, respectively, as follows:

$$\varphi = [(D_0^2 - D_1^2)] / [(D_0^2 - d^2)] \times 100\% \quad (8)$$

$$t_r = (D_0 - d) / D_0 \quad (9)$$

where D_1 represents the outer diameter after deformation and d the inner diameter of the billet. The diameter of the mandrel

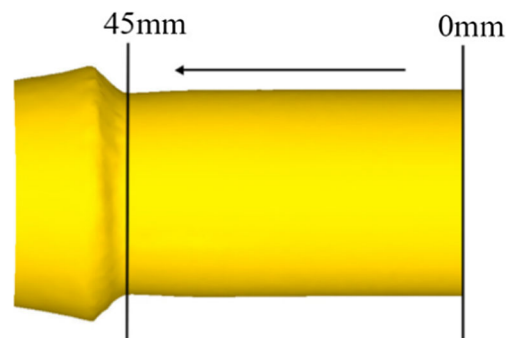
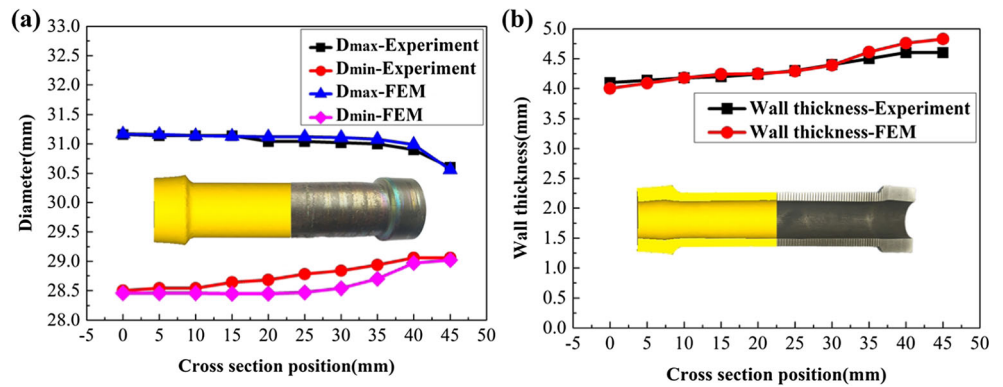


Fig. 8 Position distribution of selected cross-section

Fig. 9 Comparison of FE simulation and CWR experiment: **a** outer diameter, **b** wall thickness



is 0.5 mm smaller than the corresponding inner diameter of the billet. Corresponding with the previous isothermal compression tests, the initial deformation temperatures were selected to be in the range 850–1050 °C. The different simulation conditions are summarised in Table 2.

3.2 Finite element model

Based on DEFORM-3D, the FE model of the TC4 alloy hollow shaft in CWR with a mandrel was established, as shown in Fig. 5a. The forming process can be divided into three stages: wedging, stretching and sizing, as shown in Fig. 5b. For improving the accuracy of the simulation and the speed of the operation, the FE model was simplified based on the following assumptions: (1) the geometric symmetry and force symmetry of the workpiece were combined and half of the workpiece imposed with a symmetry constraint was simulated; (2) the workpiece was set to be plastic since its plastic deformation was considerably larger than its elastic deformation. The dies, mandrel and guide plates were defined as rigid bodies for their deformation were neglected; (3) the previously established Arrhenius-type constitutive equations were introduced to the FE model to describe the relationship between the stress, strain and temperature of the TC4 alloy; (4) the friction between the workpiece and the dies and that between the workpiece and the guide plate were constant, which were described using a shear friction model. The friction between the workpiece and the mandrel was neglected because of their

synchronous rotation; (5) the thermal effects should be considered for thermo-mechanical calculations, including the heat transfer between the workpiece and the tools, the workpiece and the mandrel, the workpiece and the guide plates, as well as the workpiece and air, as summarised in Table 3.

3.3 Cross-wedge rolling experiments

To validate the FE model of CWR and investigate the microstructure of the TC4 alloy hollow shafts in CWR, the corresponding CWR experiments were conducted under the same FE simulation conditions, as summarised in Table 2. These experiments were conducted using the H630 mill in the CWR experimental Laboratory of USTB, as shown in Fig. 6. Before deformation, each workpiece was kept in a furnace at their corresponding deformation temperatures for 30 min to ensure uniform temperature distribution. The corresponding ratio of metallographic etching agent was HF: HNO₃: H₂O = 1: 3: 16.

4 Results and discussion

4.1 Verification of the cross-wedge rolling simulation

Ellipticity is an important indicator when determining the final forming quality of hollow shafts in technical standards, as shown in Fig. 7 and described by Eq. (10).

$$e = [2 \times (D_{\max} - D_{\min}) / (D_{\max} + D_{\min})] \times 100\% \quad (10)$$

Here, D_{\max} is the maximum outer diameter of the rolled workpiece, and D_{\min} is the minimum outer diameter of the rolled workpiece.

In this section, to verify the reliability of the FE simulation, we consider as an example the CWR experiment of a hollow shaft made out of a TC4 alloy at a deformation temperature of 900 °C, forming angle of 38°, stretching angle of 4°, area reduction of 45% and relative wall thickness of 0.43. The positions investigated are at 5 mm intervals of the selected

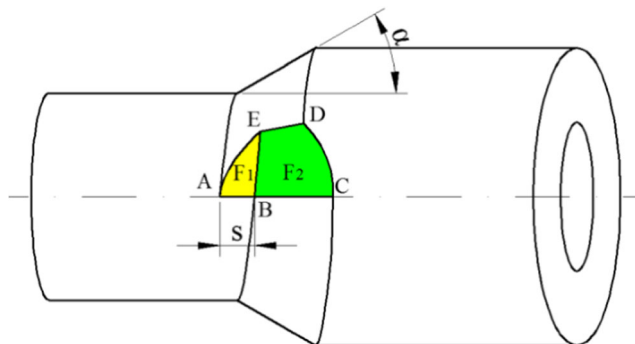
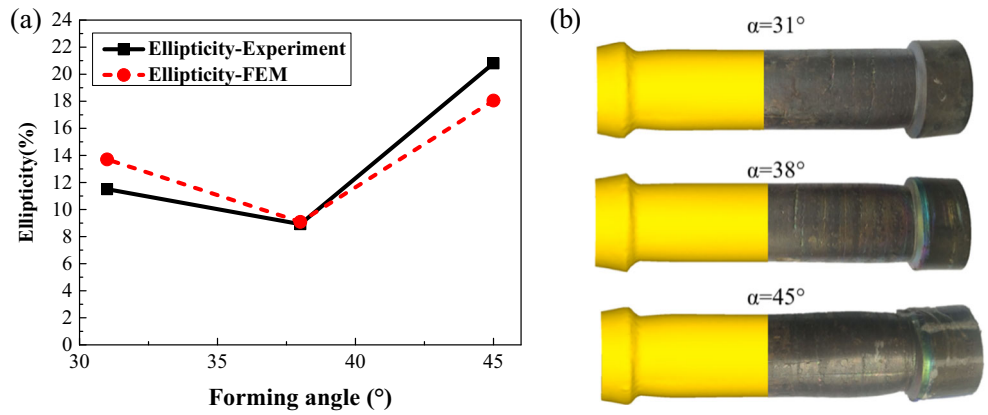


Fig. 10 Diagram of contact area between die and workpiece

Fig. 11 Effect of forming angle: **a** relationship between the ellipticity and forming angle, **b** workpieces with different forming angles



cross-sections, as shown in Fig. 8. The geometric dimensions of the TC4 alloy hollow shaft at each position are shown in Fig. 9. The errors in the maximum and minimum outer diameters are less than 0.31 mm and the wall thickness error is less than 0.23 mm, indicating that the established FE model can accurately predict the geometric dimensions of TC4 alloy hollow shafts in CWR. Moreover, it can be seen that the wall thickness distribution of the TC4 alloy hollow shaft is relatively uniform; however, the difference between the maximum diameter and the minimum diameter is large at different positions, particularly at the symmetrical section. Therefore, the ellipticity of the symmetrical plane of the rolled piece is considered as an index in this study to investigate the influence of CWR parameters on the formability of TC4 alloy hollow shafts.

4.2 Effect of process parameters on formability

The CWR process parameters affect the ellipticity of the rolled piece by changing the contact areas between the die and the workpiece. The contact areas include the arc area ABE, where the top surface of the die is in contact with the workpiece, and the spiral area BCDE, where the wedge surface of the die is contact with the workpiece [3]. The corresponding areas are denoted as F_1 and F_2 , as shown in Fig. 10. The forming angle determines the dip angle of F_2 , while the stretching angle determines the size of F_1 , because of the semicycle spread length is as follows $S = \pi(D_0 + D_1) \tan \beta/4$.

4.2.1 Effect of the forming angle

Figure 11 shows the effect of the forming angle on the ellipticity of the rolled piece at a deformation temperature of 900 °C, stretching angle of 4°, area reduction of 45% and relative wall thickness of 0.43. With an increase in the forming angle, the ellipticity first decreases and then increases.

Figure 12 shows the contact area at different forming angles. The force exerted by the spiral contact area F_2 on the rolled piece can be divided into a radial force, a tangential force and an axial force. The radial force compresses the metal, and the compressed metal flows easily along the axial direction owing to the axial force. The constant height of the top surface of the die allows the workpiece to reach the target diameter, indicating that the axial flow of the compressed metal in contact area F_1 is weak. The wall thickness of the rolled piece reduces in CWR with a mandrel, which is prone to tangential flow. A change in the forming angle can cause a change in the ratio of the radial to axial projection of the spiral contact area F_2 . An increase in the forming angle causes a relative increase in the axial force component of F_2 . Therefore, the axial force applied to the rolled piece in the forming process allows the compressed metal to realise complete axial flow, thereby reducing the tangential flow and the ellipticity. This occurs when $\tan \alpha \tan \beta < [2(D_0 - D_1)] / [\pi(D_0 + D_1)]$, as shown in Fig. 12a and b. If the increase in the forming angle meets the condition of $\tan \alpha \tan \beta > [2(D_0 - D_1)] / [\pi(D_0 + D_1)]$, the contact area worsens, as shown in Fig. 12c, because there is a rapid increase in the radial reduction of

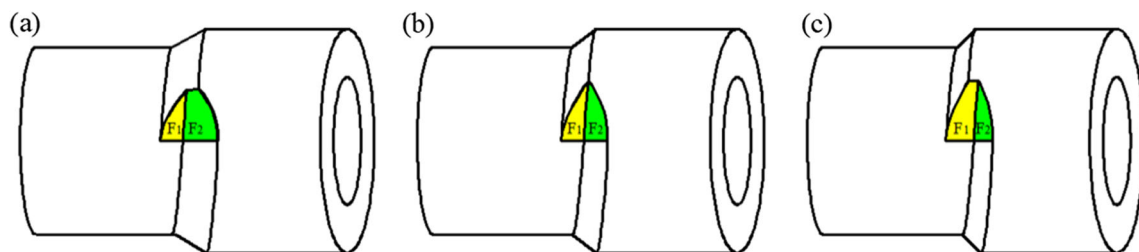
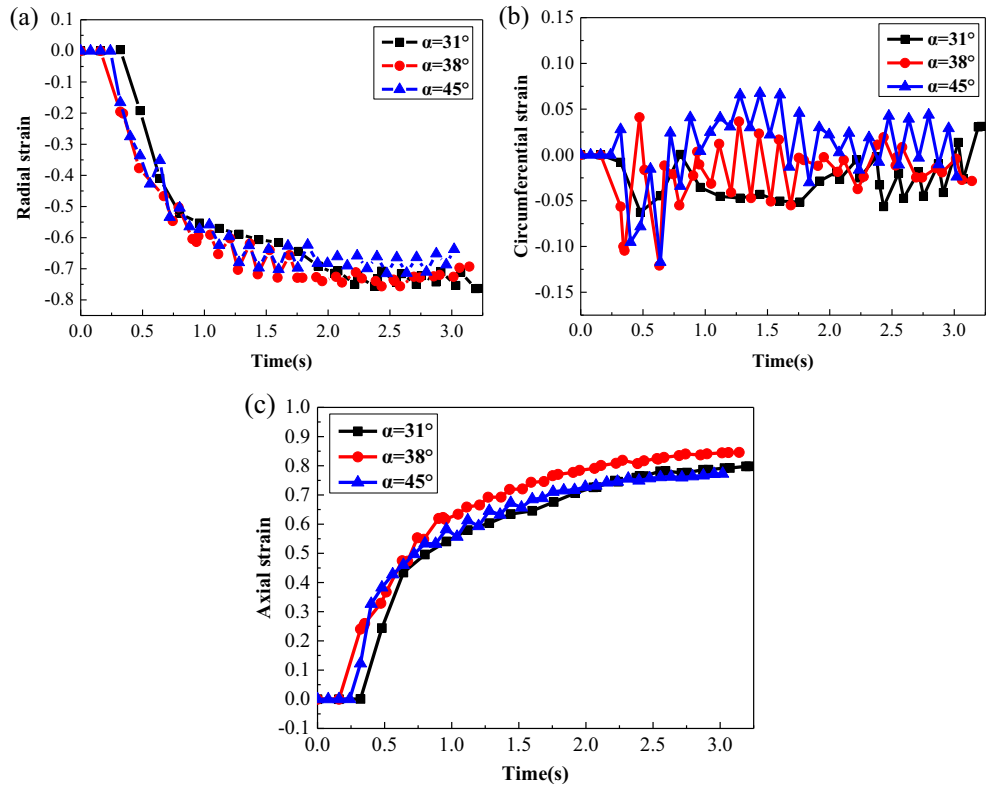


Fig. 12 Contact area at different forming angles: **a** $\alpha = 31^\circ$, **b** $\alpha = 38^\circ$, **c** $\alpha = 45^\circ$

Fig. 13 Variation in strain at different forming angles: **a** radial strain, **b** circumferential strain, **c** axial strain



F_2 , which results in an increase in flattening deformation and ellipticity.

Figure 13 shows the variation in strain at different forming angles. When the ellipticity is small (i.e. $\alpha = 38^\circ$), the radial strain exhibits a smaller fluctuation in the sizing process. The fluctuation degree reflects the ellipticity of the workpiece. The circumferential strain changes from compressive strain to tensile strain with an increase in the forming angle; however, the numerical difference is not significant under different conditions. In terms of the axial strain, a smaller ellipticity corresponds to a larger axial strain, indicating that the compressed metal achieves full axial extension. The optimal forming angle in this study is approximately 38° .

4.2.2 Effect of the stretching angle

Figure 14 shows the effect of the stretching angle on the ellipticity of the workpiece at a deformation temperature of 900°C , forming angle of 38° , area reduction of 45%, and relative wall thickness of 0.43. As the stretching angle increases, the ellipticity increases significantly.

A constant forming angle and area reduction imply that the proportional relationship between the radial force and the axial force of the spiral area F_2 is consistent. A larger stretching angle corresponds to a larger F_1 area because of the increase in S , which indicates that the axial flow of the compressed metal becomes weak. Moreover, an increase in F_1 concurrently corresponds to a larger plastic bending deformation. Therefore,

Fig. 14 Effect of stretching angle: **a** relationship between the ellipticity and stretching angle, **b** workpieces with different stretching angles

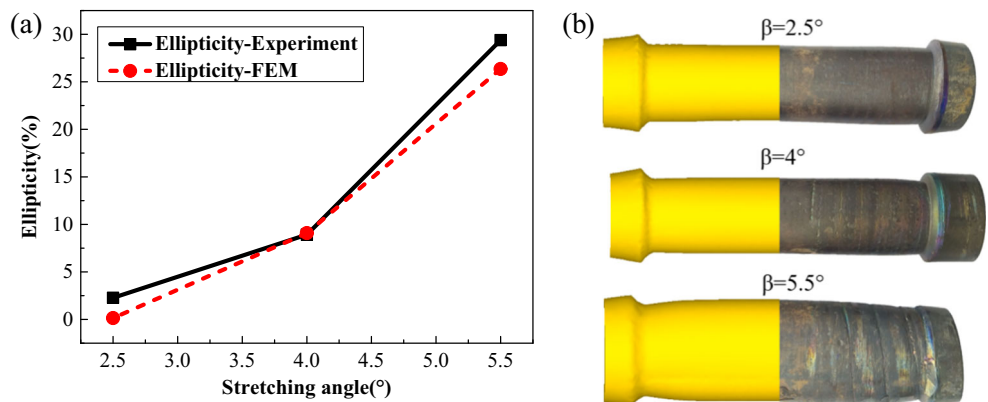
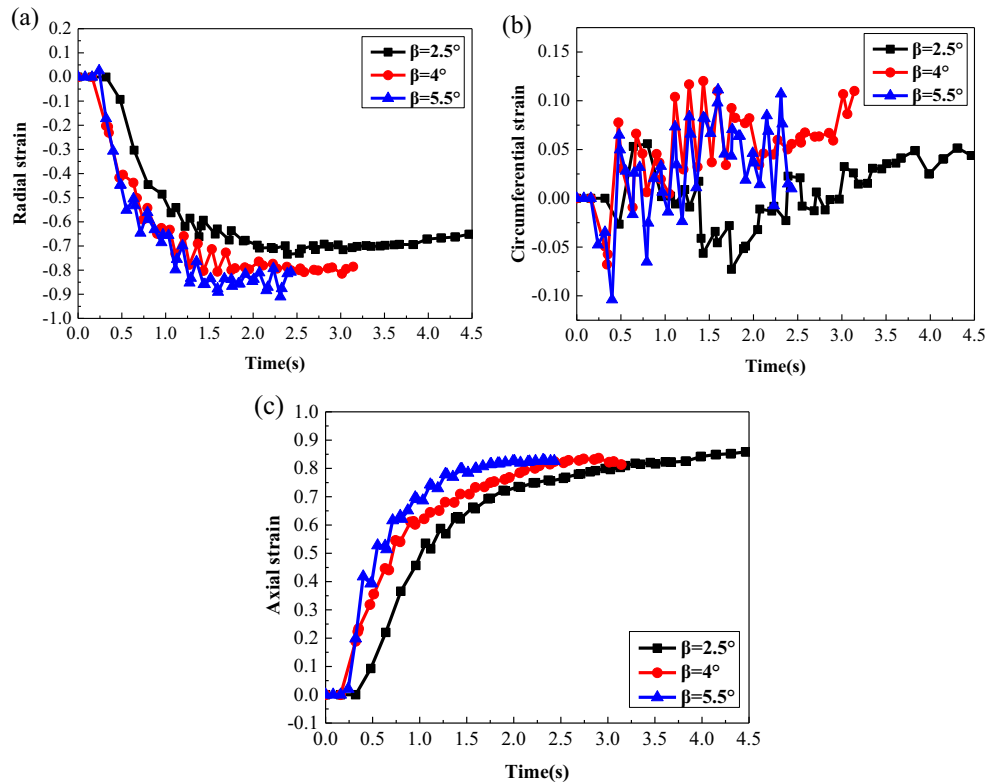


Fig. 15 Variation in strain at different stretching angles: **a** radial strain, **b** circumferential strain, **c** axial strain



the ellipticity increases considerably with an increase in the stretching angle.

Figure 15 shows the variation in strain at different stretching angles. When the stretching angle is 2.5° , the radial strain shows a small fluctuation and reaches a stable value in the sizing process. The radial strain evidently fluctuates in the entire process when the stretching angle is 5.5° . In terms of the circumferential strain, a larger stretching angle causes a larger fluctuation. The increase in axial strain during the sizing process becomes large as the stretching angle increases, which implies that the metal retained in the sizing process increases and the axial flow of metal in the main deformation process weakens. In summary, the smaller the stretching angle, the better is the forming quality of the workpiece.

4.2.3 Effect of the area reduction

Figure 16 shows the effect of area reduction on the ellipticity of the workpiece at a deformation temperature of 900°C , forming angle of 38° , stretching angle of 4° , and relative wall thickness of 0.43. The ellipticity increases first and then decreases slightly as the area reduction value increases. Under the same forming angle, the ratio of radial to axial projection of F_2 remains the same; however, the change in the area reduction value can significantly change the area ratio of F_2 and F_1 . With an increase in area reduction, the spiral area F_2 increases, which implies that the axial flow of the compressed metal is improved and the ellipticity of the rolled piece is reduced. However, increasing the area reduction value will

Fig. 16 Effect of area reduction: **a** relationship between the ellipticity and area reduction, **b** rolled pieces with different area reductions

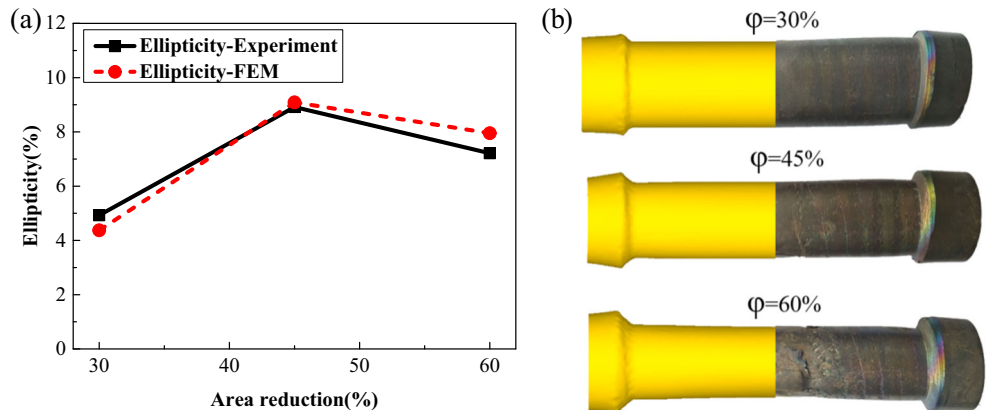
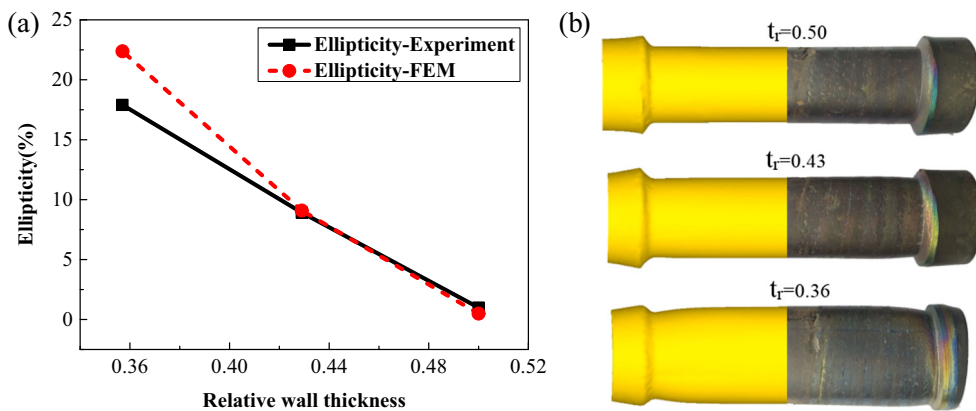


Fig. 17 Effect of wall thickness: **a** a relationship between the ellipticity and relative wall thickness, **b** rolled pieces with different wall thicknesses



cause a reduction in the wall thickness and an increase in the flattening deformation. Therefore, the influence of area reduction on the ellipticity of the rolled piece is a result of the combined action of the above two factors. Moreover, an extremely large area reduction implies a large deformation. On the one hand, this will cause necking of the rolled piece. On the other hand, it will generate a considerable heat of deformation, which makes the TC4 alloy adhere to the dies and causes a deterioration in the surface quality of the rolled piece, as shown in Fig. 16b. Therefore, when rolling the workpiece with a large area reduction value, multi-pass rolling can be adopted.

4.2.4 Effect of the wall thickness

The effect of the relative wall thickness on the ellipticity of the rolled piece at a deformation temperature of 900 °C, forming angle of 38°, stretching angle of 4°, and area reduction of 45% is shown in Fig. 17. The ellipticity evidently decreases with an increase in the relative wall thickness. This is because the flattening deformation of the workpiece decreases during the forming process as the wall thickness increases. Moreover, from Eq. (8), $(D_0^2 - D_1^2)$ will increase under the same area reduction value when the wall thickness increases, indicating that the area ratio of the spiral surface area F_2 will increase,

which improves the axial flow of the compressed metal and decreases the ellipticity.

4.2.5 Effect of the deformation temperature

Figure 18 shows the effect of the deformation temperature on the ellipticity of the rolled piece at a forming angle of 38°, stretching angle of 4°, area reduction of 45% and relative wall thickness of 0.43. The ellipticity shows a marked increase as the deformation temperature rises. For titanium alloys, the alpha phase with a close-packed hexagonal structure is harder than the beta phase with a body-centred cubic structure. The volume fraction of the beta phase increases when the temperature increases, leading to a decrease in the deformation resistance of the workpiece and an increase in the ellipticity. Furthermore, an extremely high deformation temperature can cause the TC4 alloy to adhere to the dies and degrade the surface quality of the workpiece, which should be avoided.

4.3 Effect of process parameters on microstructure

In this study, the influences of deformation temperature, area reduction and relative wall thickness on the microstructure of a TC4 titanium alloy were investigated. Figure 19a to f show the microstructure of the TC4 alloy hollow shafts under different deformation conditions. Compared with the initial

Fig. 18 Effect of the deformation temperature: **a** a relationship between the ellipticity and deformation temperature, **b** rolled pieces with different deformation temperatures

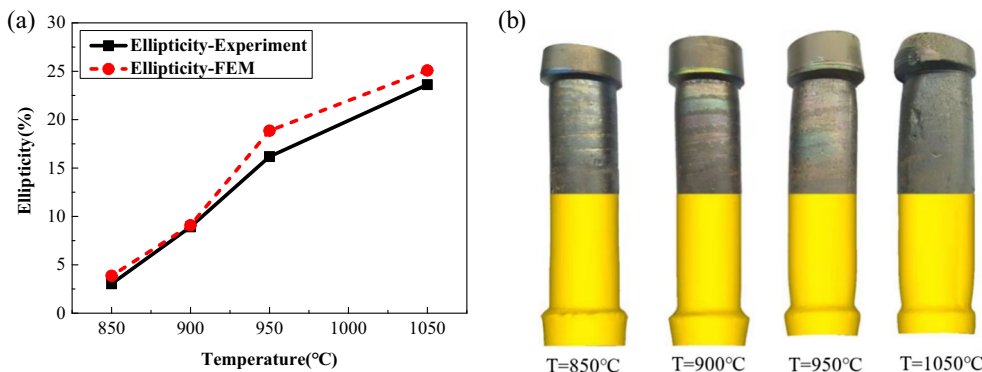
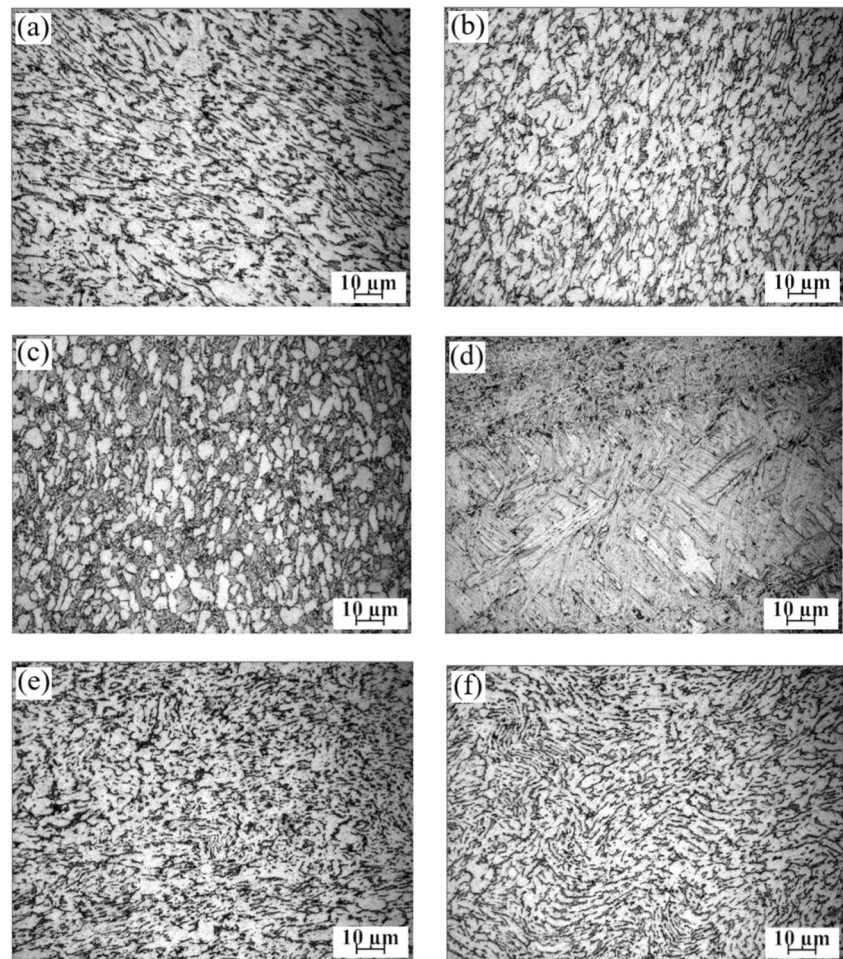


Fig. 19 Microstructure of TC4 alloy hollow shafts under different deformation conditions: **a** $T = 850$, $\varphi = 45\%$, $t_r = 0.43$; **b** $T = 900$, $\varphi = 45\%$, $t_r = 0.43$; **c** $T = 950$, $\varphi = 45\%$, $t_r = 0.43$; **d** $T = 1050$, $\varphi = 45\%$, $t_r = 0.43$; **e** $T = 900$, $\varphi = 60\%$, $t_r = 0.43$; **f** $T = 900$, $\varphi = 45\%$, $t_r = 0.50$



microstructure, it can be seen that the volume fraction of the beta phase and the morphology of the strip alpha phase evidently change with deformation temperature. The volume fraction of the beta phase increases as the temperature increases. Some of the strip alpha phase is in the kink phase state at a deformation temperature of 850 °C. When the deformation temperature is 900 °C, the degree of kink of the strip alpha phase increases, and some of the alpha phase undergoes globularisation. When the deformation temperature is 950 °C, the microstructure is composed of an equiaxed alpha phase and a transformed beta phase, which is a typical equiaxed structure. At this point, the comprehensive mechanical properties of the TC4 alloy are improved, including its plasticity, elongation, and high and low cycle fatigue strengths [18]. Miller et al. [21] and Semiatin et al. [22] indicated that the degree of kink or globularisation of the alpha platelets or the lamellar secondary alpha phase is the dominant flow softening mechanism of the TC4 alloy in the two-phase region. From Fig. 19a to c, it can be seen that increasing the deformation temperature can cause globularisation of the strip alpha phase. When the deformation temperature exceeded the beta transus temperature, all the alpha phase was transformed into

the beta phase, and the microstructure consisted of a matrix beta phase and a martensite alpha phase. With an increase in area reduction, the degree of kink of the strip alpha phase increases and the boundary of the beta phase is discontinuous owing to the large deformation, as shown in Fig. 19e. The strip alpha phase also shows an obvious kinking phase when t_r is 0.5, as shown in Fig. 19f. It can be seen that compared with the initial microstructure, the microstructure distribution of the TC4 alloy hollow shafts formed by CWR is more uniform. With the increase of initial deformation temperature, area reduction and wall thickness, the degree of kink or globularisation in the strip alpha phase increases. Especially when the deformation temperature is 950 °C, the typical equiaxed structure can be obtained.

5 Conclusions

1. The peak stress of the TC4 alloy decreases as the deformation temperature increases and the strain rate decreases, and the flow behaviour in the two-phase region shows evident flow softening. The constitutive equations of the

peak stress of the TC4 alloy in different phase regions were established.

- The ellipticity of the TC4 alloy hollow shaft decreases as the forming angle increases. However, if the forming angle meets the condition of $\tan\alpha \tan\beta > [2(D_0 - D_1)] / [\pi(D_0 + D_1)]$, the ellipticity of the hollow shaft will increase. The optimal forming angle in this study is approximately 38° .
- A larger stretching angle corresponds to a larger semicycle spread length and a larger F_1 area. Thus, the ellipticity of the TC4 alloy hollow shaft increases significantly as the stretching angle increases. When the stretching angle is 2.5° , the ellipticity of the TC4 alloy hollow shaft can be effectively decreased, which is no greater than 3%.
- The ellipticity of the TC4 alloy hollow shaft increases first and then decreases slightly as the area reduction increases. Moreover, an extremely large area reduction can increase the flattening deformation and generate considerable heat of deformation, which causes the TC4 alloy to adhere to the dies and degrades the surface quality of the rolled piece. Thus, multi-pass rolling can be used to realise a rolled piece with large area reduction.
- The flattening deformation of the workpiece decreases and the area ratio of the spiral surface F_2 increases as the relative wall thickness increases. Thus, the ellipticity of the TC4 alloy hollow shaft decreases evidently as the relative wall thickness increases.
- The ellipticity of the TC4 alloy hollow shaft shows a marked increase as the deformation temperature increases. Furthermore, an extremely high deformation temperature can also cause the TC4 alloy to adhere to the dies and degrade the surface quality of the workpiece, which should be avoided.
- The deformation temperature, area reduction and wall thickness of the workpiece have considerable effects on the microstructure of TC4 alloys in CWR. The degree of kink or globularisation in the strip alpha phase increases with an increase in the abovementioned parameters. The volume fraction of the beta phase increases with an increase in the deformation temperature. The microstructural analysis indicated a typical equiaxed structure with improved comprehensive mechanical properties at a deformation temperature of 950°C .

Acknowledgements This work is supported by the Aeronautical Science Foundation of China (Grant No. 20173674003), the National Natural Science Foundation of China (Grant No. 51875036), and the Engineering Research Center of Part Near-Net-Shape forming of Ministry of Education.

Author contribution Pengni Feng: conceptualization, investigation, methodology, data curation, writing—original draft, reviewing and editing.

Cuiping Yang: supervision, conceptualization, methodology, resources, funding acquisition, reviewing and editing.

Baoyu Wang: supervision, conceptualization, methodology, funding acquisition, reviewing and editing.

Junling Li: supervision, methodology, reviewing and editing.

Jinxia Shen: supervision, methodology, reviewing and editing.

Xiaoming Yang: supervision, reviewing and editing.

Data availability The datasets generated and/or analysed during the current study are available from the corresponding author on reasonable request.

Declarations

Ethics approval and consent to participate The article follows the guidelines of the Committee on Publication Ethics (COPE) and involves no studies on human or animal subjects.

Consent for publication Applicable.

Conflict of interest The authors declare no conflict of interest.

References

- Boyer RR (1995) Titanium for aerospace: rationale and applications. *Adv Perform Mater* 2:349–368. <https://doi.org/10.1007/BF00705316>
- Li MQ, Li H, Luo J (2016) Precision forging of titanium alloy. Science Press, Beijing (in Chinese)
- Hu ZH, Zhang KS, Wang BY, Zhang W (1996) Theory and application of cross wedge rolling. Metallurgical Industry Press, Beijing (In Chinese)
- Bartnicki J, Pater Z (2004) The aspects of stability in cross-wedge rolling processes of hollow shafts. *J Mater Process Technol* 155–156:1867–1873. <https://doi.org/10.1016/j.jmatprotec.2004.04.278>
- Bartnicki J, Pater Z (2005) Numerical simulation of three-rolls cross-wedge rolling of hollow shaft. *J Mater Process Technol* 164–165:1154–1159. <https://doi.org/10.1016/j.jmatprotec.2005.02.120>
- Ding W, Zhang KS, Yang CP, Hu ZH (2010) Study on the ovality of hollow shafts with equal inner diameter formed by cross wedge rolling. *J Plast Eng* 17:27–31. (in Chinese). <https://doi.org/10.3969/j.issn.1007-2012.2010.03.006>
- Yang CP, Hu ZH (2014) Influence of flattening deformation on the forming of hollow parts in cross-wedge rolling. *Trans Beijing Inst Technol* 34:881–885 (in Chinese)
- Yang CP, Hu ZH (2015) Research on the ovality of hollow shafts in cross wedge rolling with mandrel. *Int J Adv Manuf Technol* 83:67–76. <https://doi.org/10.1007/s00170-015-7478-3>
- Ji HC, Liu JP, Wang BY, Zheng ZH, Huang JH, Hu ZH (2015) Cross wedge rolling of a 4Cr9Si2 hollow valve: explorative experiment and finite element simulation. *Int J Adv Manuf Technol* 77: 15–26. <https://doi.org/10.1007/s00170-014-6363-9>
- Ji HC, Liu JP, Wang BY, Fu XB, Xiao WC, Hu ZH (2017) A new method for manufacturing hollow valves via cross wedge rolling and forging: Numerical analysis and experiment validation. *J Mater Process Technol* 240:1–11. <https://doi.org/10.1016/j.jmatprotec.2016.09.004>
- Huang X, Wang BY, Mu YH, Shen JX, Li JL, Zhou J (2019) Investigation on the effect of mandrels on hollow shafts in cross-wedge rolling. *Int J Adv Manuf Technol* 102:443–455. <https://doi.org/10.1007/s00170-018-3093-4>

12. Urankar S, Lovell M, Morrow C, Li Q, Kawada K (2006) Establishment of failure conditions for the cross-wedge rolling of hollow shafts. *J Mater Process Technol* 177:545–549. <https://doi.org/10.1016/j.jmatprotec.2006.04.052>
13. Urankar S, Lovell M, Morrow C, Li Q, Kawada K (2006) Development of a critical friction model for cross wedge rolling hollow shafts. *J Mater Process Technol* 177(1–3):539–544. <https://doi.org/10.1016/j.jmatprotec.2006.04.048>
14. Çakırcalı M, Kılıçaslan C, Güden M, Kıranlı E, Shchukin VY, Petronko VV (2013) Cross wedge rolling of a Ti6Al4V (ELI) alloy: the experimental studies and the finite element simulation of the deformation and failure. *Int J Adv Manuf Technol* 65:1273–1287. <https://doi.org/10.1007/s00170-012-4256-3>
15. Li JL, Wang BY, Ji HC, Huang X, Tang XF, Ma WP (2017) Effects of the cross-wedge rolling parameters on the formability of Ti-6Al-4V alloy. *Int J Adv Manuf Technol* 92:2217–2229. <https://doi.org/10.1007/s00170-017-0263-8>
16. Li JL, Wang BY, Ji HC, Zhou J, Fu XB, Huang X (2018) Numerical and experimental investigation on the cross wedge rolling of powder sintering TC4 alloy. *Int J Adv Manuf Technol* 94:2149–2162. <https://doi.org/10.1007/s00170-017-0992-8>
17. Li JL, Wang BY, Qin Y, Fang S, Huang X, Chen P (2019) Investigating the effects of process parameters on the cross wedge rolling of TC6 titanium alloy based on temperature and strain rate sensitivities. *Int J Adv Manuf Technol* 103:2563–2577. <https://doi.org/10.1007/s00170-019-03461-3>
18. Zhao YQ, Chen YN, Zhang XM, Zeng XD, Wang L (2012) Phase transformation and heat treatment of titanium alloys. Central South University Press, Changsha (in Chinese)
19. Ding R, Guo ZX, Wilson A (2002) Microstructural evolution of a Ti-6Al-4V alloy during thermomechanical processing. *Mater Sci Eng A* 327:233–245. [https://doi.org/10.1016/S0921-5093\(01\)01531-3](https://doi.org/10.1016/S0921-5093(01)01531-3)
20. Bai Q, Lin JG, Dean TA, Balint DS, Gao T, Zhang Z (2013) Modelling of dominant softening mechanisms for Ti-6Al-4V in steady state hot forming conditions. *Mater Sci Eng A* 559:352–358. <https://doi.org/10.1016/j.msea.2012.08.110>
21. Miller RM, Bieler TR, Semiatin SL (1999) Flow softening during hot working of Ti-6Al-4V with a lamellar colony micro-structure. *Scr Mater* 40:1387–1393. [https://doi.org/10.1016/S1359-6462\(99\)00061-5](https://doi.org/10.1016/S1359-6462(99)00061-5)
22. Semiatin SL, Seetharaman V, Weiss I (1999) Flow behavior and globularization kinetics during hot working of Ti-6Al-4V with a colony alpha microstructure. *Mater Sci Eng* 263:257–271. [https://doi.org/10.1016/S0921-5093\(98\)01156-3](https://doi.org/10.1016/S0921-5093(98)01156-3)

Publisher's note Springer Nature remains neutral with regard to jurisdictional claims in published maps and institutional affiliations.